Title

Crystallization of Brome Mosaic Virus and T = 1 Brome Mosaic Virus Particles Following a Structural Transition

Journal

Virology, 286(2)

ISSN

0042-6822

Authors

Lucas, Robert W
Kuznetsov, Yurii G
Larson, Steven B
et al.

Publication Date

2001-08-01

DOI

10.1006/viro.2000.0897

Virology **286,** 290–303 (2001)
doi:10.1006/viro.2000.0897, available online at http://www.idealibrary.com on IDEAL®

Crystallization of Brome Mosaic Virus and $T = 1$ Brome Mosaic Virus Particles Following a Structural Transition

Robert W. Lucas, Yurii G. Kuznetsov, Steven B. Larson, and Alexander McPherson[1]

University of California, Irvine, Department of Molecular Biology and Biochemistry, Irvine, California 92697-3900

Received November 9, 2000; returned to author for revision January 17, 2001; accepted March 6, 2001

Brome mosaic virus (BMV), a $T = 3$ icosahedral plant virus, can be dissociated into coat protein subunits and subunit oligomers at pH 7.5 in the presence of concentrated salts. We have found that during the course of this treatment the coat protein subunits are cleaved, presumably by plant cell proteases still present in the preparation, between amino acids 35 and 36. The truncated protein subunits will then reorganize into $T = 1$ icosahedral particles and can be crystallized from sodium malonate. Quasi elastic light scattering and atomic force microscopy results suggest that the transition from $T = 3$ to $T = 1$ particles can occur by separate pathways, dissociation into coat protein subunits and oligomers and reassembly into $T = 1$ particles, or direct condensation of the $T = 3$ virions to $T = 1$ particles with the shedding of hexameric capsomeres. The latter process has been directly visualized using atomic force microscopy. Native $T = 3$ virions have been crystallized in several different crystal forms, but neither a rhombohedral form nor either of two orthorhombic forms diffract beyond about 3.4 Å. Tetragonal crystals of the $T = 1$ particles, however, diffract to at least 2.5 Å resolution. Evidence suggests that the $T = 1$ particles are more structurally uniform and ordered than are native $T = 3$ virions. A variety of anomalous virus particles having diverse sizes have been visualized in preparations of BMV used for crystallization. In some cases these aberrant particles are incorporated into growing crystals where they are frequently responsible for defect formation.

INTRODUCTION

Brome mosaic virus (BMV) is the type member of the bromoviridae family and bromovirus genus (Van Regenmortel *et al.,* 1999). It has a tripartite, positive-sense, single-stranded genome with sizes of 3.2, 2.8, and 2.1 kb for RNA1, RNA2, and RNA3, respectively, and a commonly occurring 800 base fragment, RNA4, which contains only the gene for the coat protein (Pirone and Shaw, 1990). BMV forms $T = 3$ virions of 28 nm *in vivo* that consist of 180 identical copies of the coat protein that assume three slightly altered conformations in the capsid. Similar to Cowpea chlorotic mottle virus (CCMV) (Bancroft, 1971), which it resembles, it has been the focus of a wide variety of physical–chemical techniques, too extensive to be detailed, but reviewed elsewhere (Argos and Johnson, 1984; Bancroft and Horne, 1977; Lane, 1981).

It is relevant to the investigation presented here to note that BMV is most stable at pH 4.5 at low-to-moderate ionic strength, but even then appears somewhat heterogeneous in its size and properties (Argos and Johnson, 1984). At pH 7.5 or higher, and at 0.5 M or higher ionic strength, it is reported to dissociate into dimers (Cuillel *et al.,* 1981). Upon reestablishment of low pH and ionic strength, reassociation occurs, but a great variety of products are apparently possible. Under defined conditions, BMV or CCMV have been known to form sheets, tubes, empty $T = 3$ particles, $T = 2$ particles, aggregates of coat protein, multishelled capsids, ellipsoids, small particles, and other aberrant forms (Bancroft *et al.,* 1967, 1969; Krol *et al.,* 1999; Pfeiffer *et al.,* 1976; Pfeiffer and Hirth, 1974).

It is also reported that if the dissociated virions are treated with trypsin so that the 64 amino acids at the N-terminus are removed from the capsid proteins, then reassociation results in $T = 1$ particles (Cuillel *et al.,* 1981). These particles are a point of special interest here, as we have, it seems, obtained similar particles without deliberate addition of protease.

From the available evidence, BMV is among the most structurally versatile of the icosahedral plant viruses. As such, it has provided an unusually good subject for the study of assembly and disassembly, and the role of various structural and chemical factors in those processes. With that in mind, we initiated X-ray crystallographic, atomic force microscopy (AFM), and quasi elastic light scattering studies (QELS) of BMV to better define the structural bases for the observed phenomena.

RESULTS

Formation of T = 1 particles

SDS–PAGE of native BMV preparations showed only a single band on gels, and this appeared at a molecular

[1] To whom correspondence and reprint requests should be addressed. Fax: (949) 824-1954. E-mail: amcphers@uci.edu.

0042-6822/01 $35.00

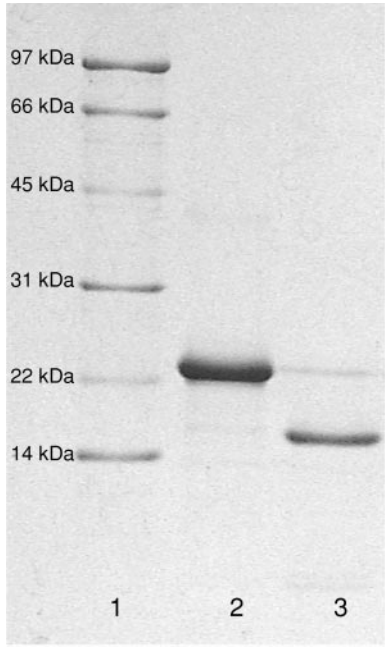

FIG. 1. SDS–PAGE of BMV and $T = 1$ BMV particles. In lane 1 are molecular weight standards; lane 2, intact BMV; and lane 3, the protein comprising the $T = 1$ particles.

weight consistent with that of the coat protein. Mass spectrometry yielded a value of 20,346 Da for the intact BMV which very closely corresponds to the expected mass of 20,385 Da for the BMV coat protein. Only a single prominent peak was observed, consistent with SDS–PAGE, indicating that coat protein subunits on virtually all virions were completely intact. SDS–PAGE of the BMV after exposure to high salt, presented in Fig. 1, clearly showed that the only species present was not intact protein, but a polypeptide of about $M_r = 16{,}500$. Mass spectrometry analyses of the BMV after exposure to high salt yielded a mass value of 16,462 Da. Again, only a single prominent peak was in evidence.

The latter result clearly indicated that the coat protein, which reassembled into $T = 1$ particles, was cleaved. Amino-terminal sequencing of the salt-treated protein revealed only a single amino terminus present in the preparation, and this had the sequence AAGQGK-. This sequence corresponds uniquely to amino acids 36–41 of the BMV coat protein and indicates that cleavage occurs between amino acids leucine 35 and alanine 36. Loss of the amino-terminal peptide 1–35 would yield a mass for the remaining protein of 16,449, which is consistent with the value observed by mass spectrometry.

Because no protease was added to the $CaCl_2$–BMV solution during dissociation, an attempt was made to identify the (presumably) enzymatic source of the cleavage in the BMV coat protein. The most likely possibilities were impurities in the BMV preparation itself, most probably from the host plant (barley) cells, and possibly from the RNase A that was added. To assess this latter possibility, BMV was treated as above with $CaCl_2$ in the presence and absence of RNase A, but in both cases also in the presence of 3 mM p-methyl sulfonyl fluoride (PMSF). The PMSF was well in excess of that needed to irreversibly inhibit any trace serine proteases in either the virus preparation itself or the preparation plus added RNase. No difference in the cleavage pattern was observed whether RNase A or PMSF was present. This demonstrated that cleavage was not produced by a serine protease, nor by a contaminant of the RNase A. Though we did not attempt to quantitate it, we did observe that in the presence of RNase A cleavage of the coat protein, even with PMSF or other inhibitors present, appeared to be significantly accelerated.

X-ray crystallography

A number of crystal forms, some shown in Fig. 2, appeared in the course of identifying conditions for nucleation and growth, and many were examined for their diffraction properties. Several yielded only very low resolution diffraction data and were pursued no further. Other forms, however, produced diffraction patterns that we are confident will be adequate for structure determination. The characteristics of the various crystal forms are presented in Table 1. It is noteworthy that while none of the crystal forms of the native $T = 3$ virus diffract to beyond about 3.4 Å resolution, the crystals of the $T = 1$ particles diffract to at least 2.5 Å, and they consistently demonstrate a significantly lower mosaicity. A diffraction comparison of crystals of the native virus and the $T = 1$ particle crystals are shown in Fig. 3.

AFM investigation

Both the orthorhombic and rhombohedral crystals of BMV were examined in their mother liquors using AFM. The crystals of the latter form, seen in Fig. 2b, were rather soft, but nonetheless permitted imaging at lattice resolution. The orthorhombic crystals in Fig. 2a, on the contrary, were physically firm and more amenable to AFM analysis. The orthorhombic lattice is clearly evident in low-resolution images similar to those in Fig. 4a. Even moderate resolution images as in Fig. 4b contain some virion structural information.

High-resolution AFM images of the orthorhombic form, similar to those in Fig. 5, are revealing and clearly show the organization of capsomeres on the surfaces of the viral particles. The distinctive appearance of the virions and the capsomeres are perceptively different from previously observed for Turnip Yellow Mosaic Virus (TYMV), a $T = 3$ tymovirus (Malkin *et al.,* 1999a). In TYMV the capsomeres were less open but far more protruding. The views in Fig. 5 are roughly along threefold (quasi sixfold) axes so that the particles exhibit a hexagonal outline. One can see that the particles comprising adjacent vertical rows are inclined with respect to one another: one

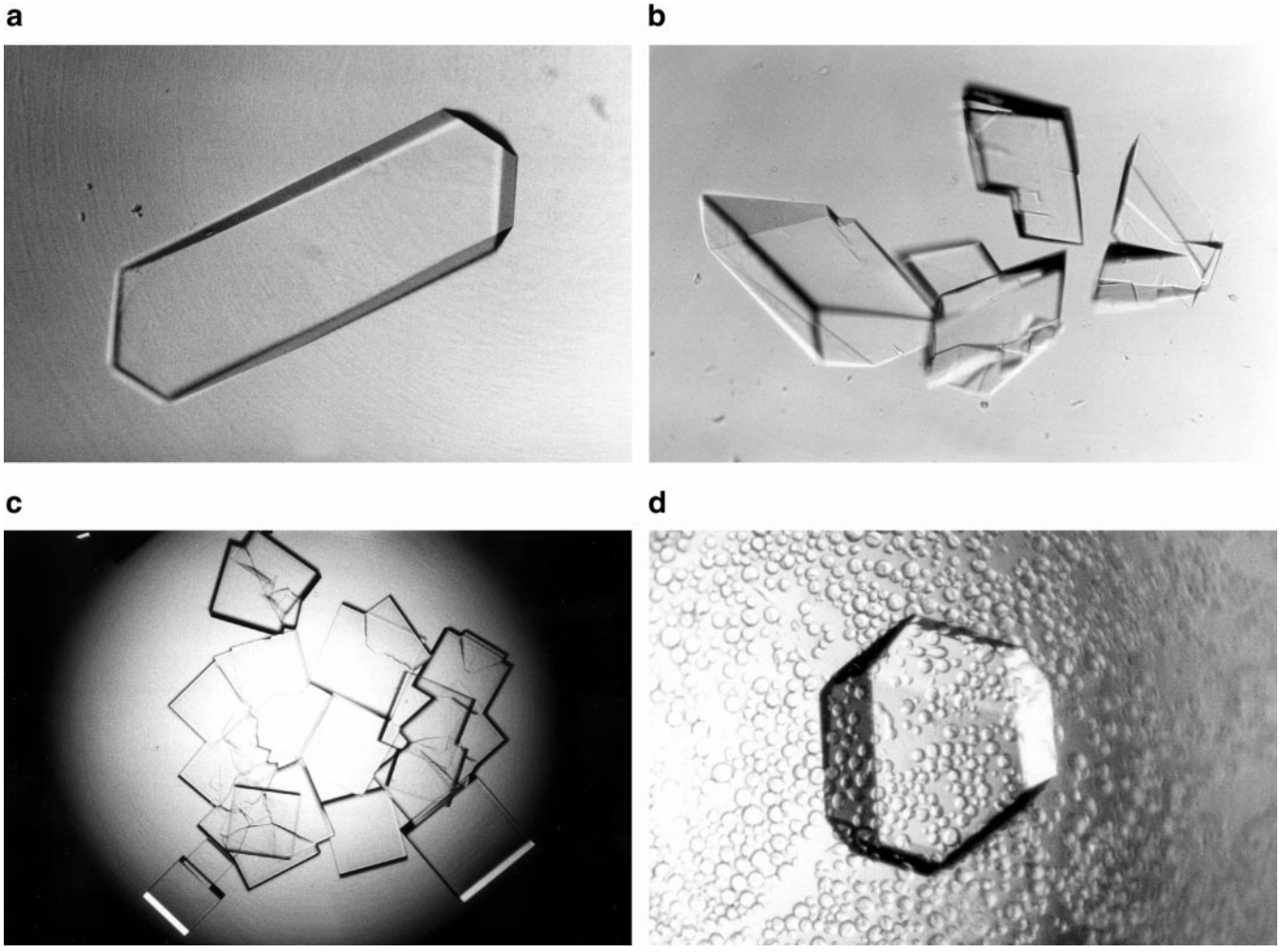

FIG. 2. In (a), a low-magnification light micrograph of an orthorhombic crystal of native BMV (space group $C222_1$), approximately 1.5 mm in length. In (b) are rhombohedral crystals (R3) and in (c) crystals of a second orthorhombic crystal form ($P2_12_12_1$), also of native $T = 3$ BMV. In (d) is a polygonal crystal of the tetragonal form of the $T = 1$ particles of BMV formed by exposure to $CaCl_2$ and crystallized from sodium malonate.

column "looking up," and the next column "looking down." This arrangement is consistent with a 2_1 screw axis in the plane of the image and with the orthorhombic symmetry of the crystal as deduced by X-ray diffraction (see Table 1).

The BMV crystals, both orthorhombic and rhombohedral, are of some interest from the perspective of crystal growth and perfection. From previous work we know that the BMV crystals grow by two-dimensional nucleation. We have not, to this point, observed any screw dislocations. We also see no stacking faults (Malkin *et al.,* 1995, 1996). A large number of point defects are present, however, and the absence of particles from lattice points is clearly evident over the entire surface of the crystal. These vacancies are not later filled, but remain empty lattice sites. Often several absences occur along a line or as a small group, thereby producing larger cavities.

Some of the defects produced in the surface are revealing. In images of the rhombohedral crystals in Fig. 6, it can be seen that, in addition to the 28-nm $T = 3$ BMV particles, the lattice also occasionally contains anomalous, small particles as well. The diameter of these "small particles" is about 17–18 nm, that of a $T = 1$ icosahedral particle. This implies that not only are $T = 1$ BMV particles occasionally present in the preparations of native BMV used in crystallization, but that they can form sufficient crystallographic interactions to allow them to be incorporated, albeit with defect creation, into the $T = 3$ BMV crystal lattice.

In Fig. 6 it can also be seen that at the edges of somewhat more extensive defects, where large groups of lattice points are empty, anomalously larger particles are also incorporated into the crystal lattice. Although these larger particles produce even greater perturbations to the lattice, and greater defect size, they form enough legitimate crystallographic interactions with neighbors to gain acceptance to the crystal. From the images we estimate the diameters of these larger parti-

TABLE 1

BMV Crystal Characteristics

	Cell dimensions	Temperature	Diffraction resolution	Particles per unit cell	Position of particle center	Asymmetric unit
T = 3 Particle crystal space groups						
$C222_1$	a = 552 Å b = 745 Å c = 270 Å	22°C	3.9 Å	8	General	1 Particle
R3	a = b = c = 265 Å $\gamma = 61.4°$					
	(H3, a = b = 271 Å c = 646 Å)	−173°C	3.6 Å	1	On threefold axis	$\frac{1}{3}$ Particle
$P2_12_12_1$	a = 367 Å b = 377 Å c = 414 Å	22°C	3.5 Å	4	General	1 Particle
T = 1 Particle crystal space groups						
$P4_122$ or $P4_322$	a = b = 193.7 Å c = 428.3 Å	−173°C	2.5 Å	4	On twofold axis	$\frac{1}{2}$ Particle
P222	a = 183 Å b = 189 Å c = 218 Å	−173°C	2.5 Å	2	On twofold axis	$\frac{1}{2}$ Particle

cles to be about 38–40 nm. These could be icosahedrons of a higher T value, or they may be double-shelled virions, such as previously reported (Bancroft and Hiebert, 1967; Bancroft *et al.,* 1967).

We modeled the field of virus particles comprising the surfaces of the rhombohedral crystals (the equivalent 100, 010, and 001 faces) in the following way. Our initial model for BMV structure solution, which is CCMV mutated to the BMV sequence, was created as an accessible surface representation using the program GRASP (Nicholls *et al.,* 1991). It was placed in an orientation such that an icosahedral threefold axis was coincident with

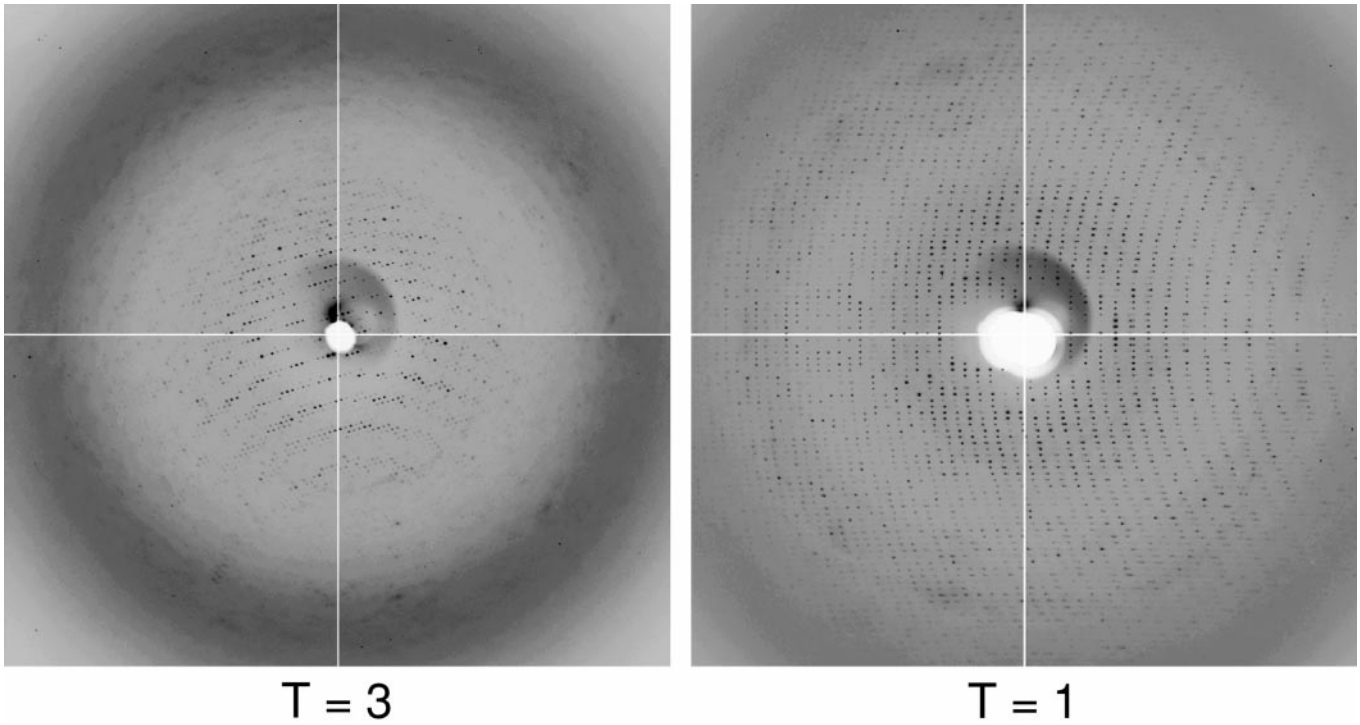

FIG. 3. In (a) is a 0.5° oscillation image from the diffraction pattern of the rhombohedral crystal form of native $T = 3$ BMV. It exhibits a resolution limit of about 3.8 Å. In (b), an equivalent image is taken from the diffraction pattern of a tetragonal crystal of the $T = 1$ BMV particles, showing a diffraction limit of about 2.5 Å.

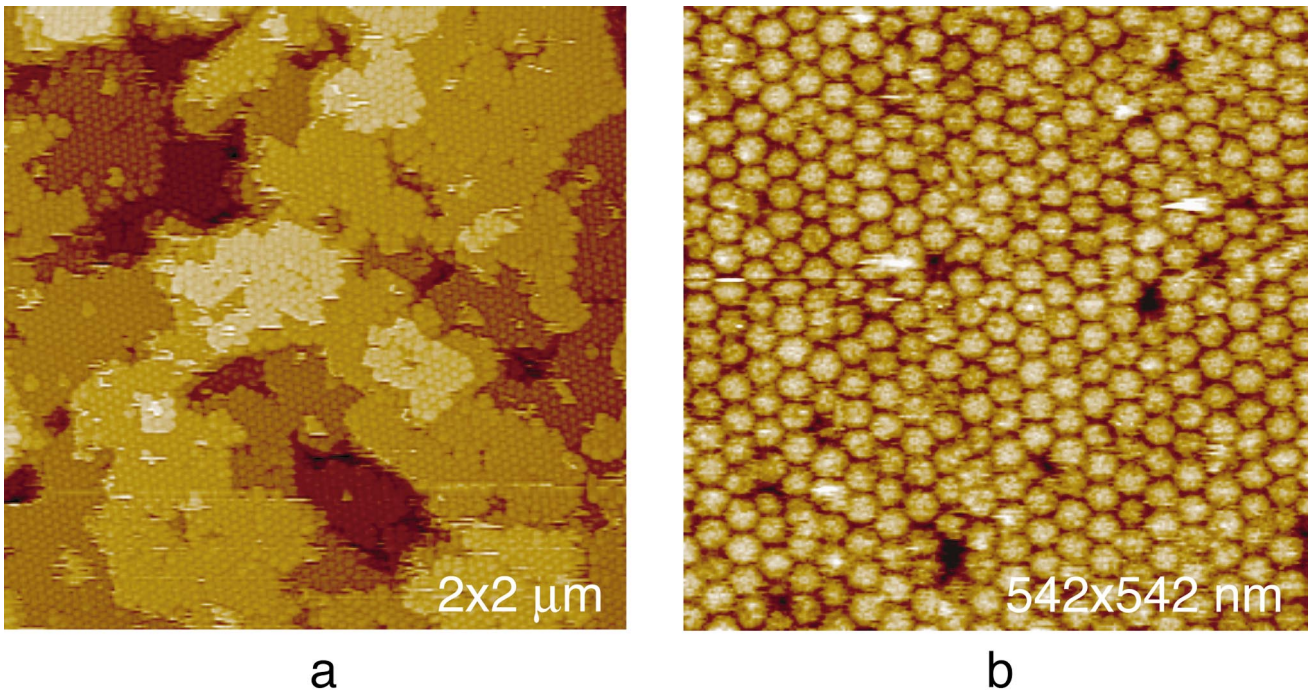

FIG. 4. In (a) a low magnification atomic force microscope (AFM) image shows the two-dimensional growth islands that characterize the surfaces of orthorhombic $T = 3$ BMV crystals. In (b) is a high-magnification AFM image of the surface of an orthorhombic $T = 3$ BMV crystal. As with most virus crystals, and indeed most macromolecular crystals in general, many absences are present over the surface, and in (a) vacancies frequently occur in clusters to produce larger defects. In (b) even at this relatively modest magnification, the capsomeric structure of the viral surfaces is emerging.

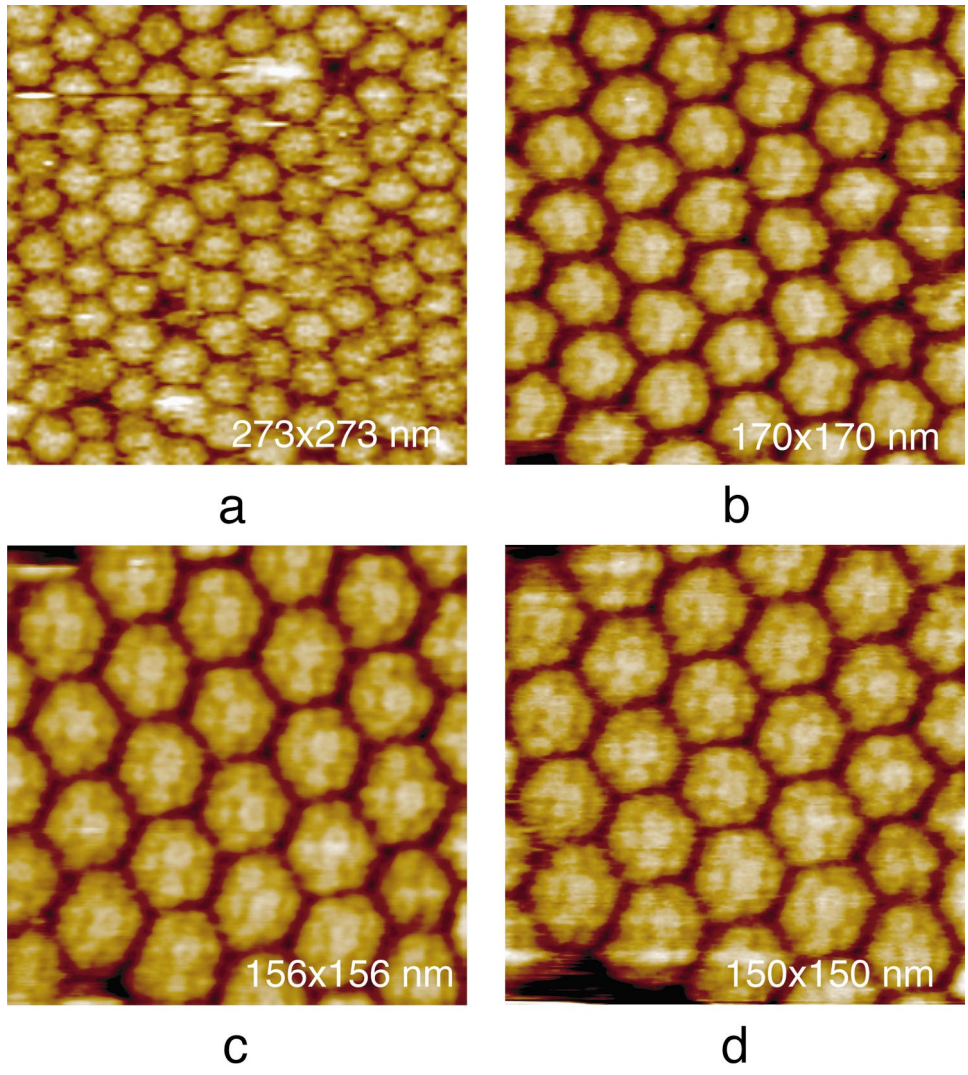

FIG. 5. In (a) through (d) are high-magnification images of the surfaces of orthorhombic $T = 3$ BMV crystals where the capsomeres are frequently visible on individual virions. The areas scanned in (c) and (d) are identical, but the scanning was done in the vertical direction in (c) and the horizontal direction in (d), which gives some measure of the distortion introduced by the scan direction.

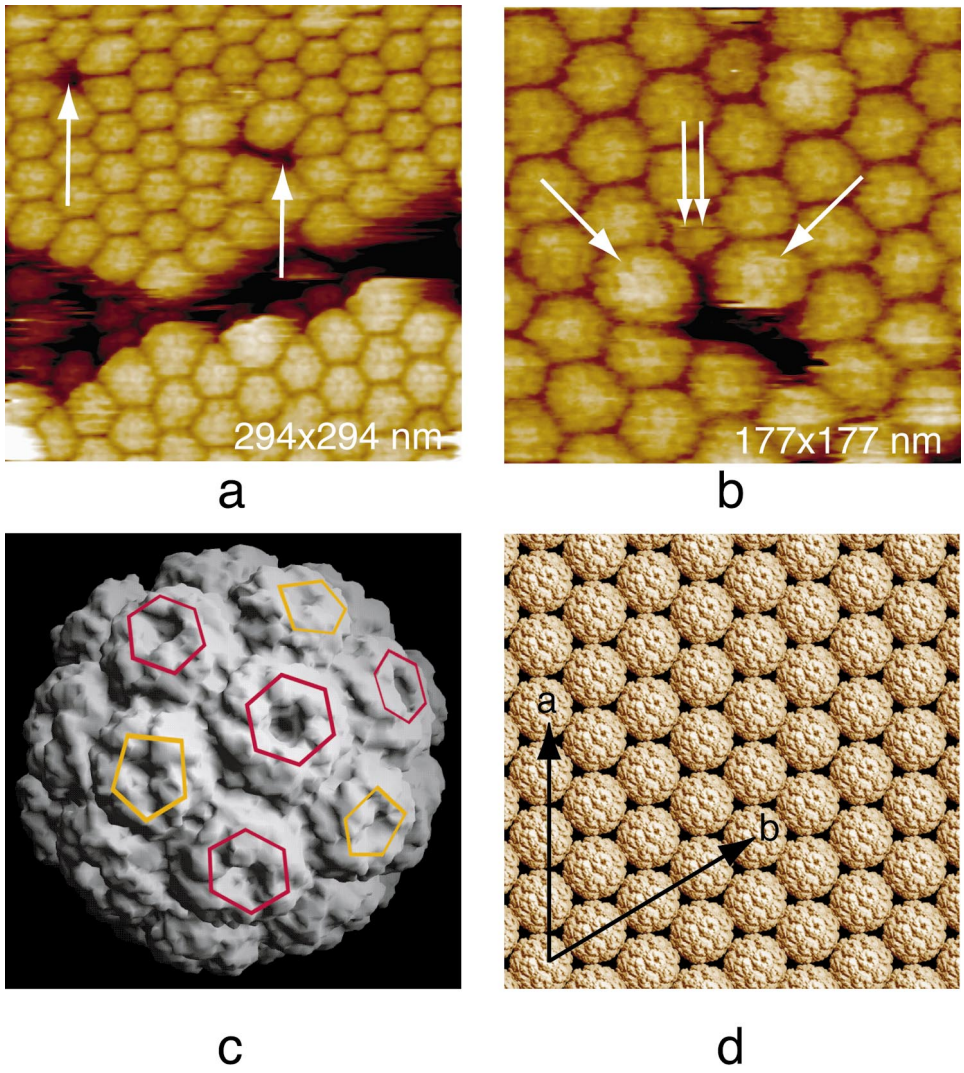

FIG. 6. An AFM image of a small area on the surface of a rhombohedral $T = 3$ BMV crystal is shown in (a), which contains a defect between two step edges, and a minor defect marked by arrows. In (b) this minor defect is shown at higher magnification, revealing the source. Two viral particles of abnormally large size, about 36 nm diameter, have been incorporated into the lattice along with an aberrant small particle (both marked with arrows and double arrows), probably a $T = 3$ particle, all adjacent to one another. The set of aberrant particles precludes normal lattice formation and the local stress is accommodated by formation of the empty space in the crystal. Near the top of the image, again marked with arrows, is a small particle incorporated adjacent to a large aberrant particle. Here the combination of a large and a small particle apparently self-compensates and allows propagation of the lattice without serious defect creation. In (c) the starting model for structure determination, CCMV mutated to the BMV sequence, has been placed in an orientation consistent with the rotation function and in (d) unit cell translations applied to simulate the 001 face of the rhombohedral crystal seen in (a) and (b). Hexagonal capsomeres are indicated in red in (c), and pentameric capsomeres in yellow.

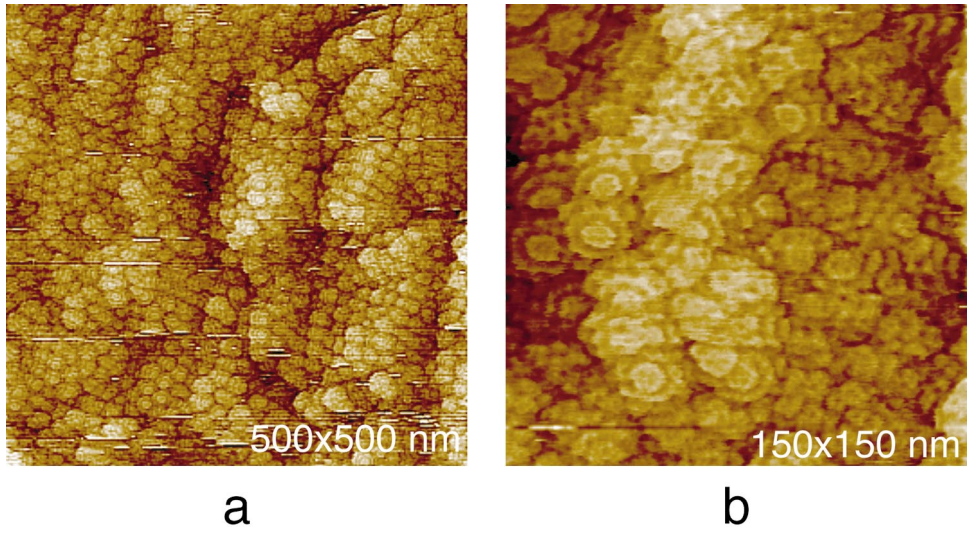

FIG. 7. Successively higher magnification AFM images of the surfaces of a tetragonal $T = 1$ BMV particle crystal which is undergoing dissolution and disgorging masses of the $T = 1$ particles. Close inspection shows the particles to have assumed many different orientations as they are freed from the crystals, thereby showing capsids in disparate views.

the crystallographic threefold axis. It was then rotated about the threefold axis according to the rotation function solution to yield the perspective seen in Fig. 6c. The entire surface was then generated by translating the particle, in that orientation, in a periodic manner by the rhombohedral unit cell lengths. The resultant model surface is shown in Fig. 6d. It compares well, we believe, with the rhombohedral crystal faces observed by AFM and shown in Figs. 6a and 6b.

We initially experienced some technical difficulties in visualizing the crystals of $T = 1$ BMV particles in their malonate mother liquor and could only image them under conditions where partial dissolution had occurred. This so disordered the crystal surface that the lattice was no longer evident, but many particles at the surface were, nonetheless, still relatively immobilized by crystal interactions. Images, similar to those in Fig. 7, provided some informative views of individual particles in a variety of different orientations. Even in these images, prominent capsomeres, rosette in form, are seen to protrude from and to decorate the particles which have diameters of 18 nm.

We eventually found that if the $T = 1$ BMV crystals grown from 2.1 M malonate were washed for several minutes in 3 M ammonium sulfate before imaging, the crystals were stable and their surfaces clean. From these washed crystals, images similar to those in Fig. 8 were obtained, and these, at higher resolution, show even more clearly the features of the $T = 1$ particles. Again, the rosette capsomeres protruding from the particle surfaces are apparent, but in addition, the capsomeres have visible depressions, or holes of 2 to 3 nm at their centers. The capsomeres of the $T = 3$ particles closely resemble those recorded on the surfaces of native $T = 3$ virions and are probably the same.

To investigate the formation of $T = 1$ particles derived from native $T = 3$ BMV, we attempted to replicate the procedure used to produce the free coat protein for crystallization, but in the AFM fluid cell. We assumed that the transition from $T = 3$ to $T = 1$ likely occurred by one of two mechanisms. The first would require complete disassembly of the $T = 3$ particles into protein units (monomers, dimers, pentamers, hexamers) and their reassembly into $T = 1$ particles. A second mechanism might involve a direct condensation of $T = 3$ to $T = 1$ particles by shedding of hexameric capsomeres. Both mechanisms could also be operative simultaneously.

Figure 9 illustrates the results of the experiment. In (a) native $T = 3$ BMV particles have been adsorbed to freshly cleaved mica in a buffer solution. They all have diameters determined from height measurements to be 27–29 nm. In (b) $CaCl_2$ has begun diffusing into the fluid cell from feed lines (producing the interference seen at the bottom of the image), and (c–f) are sequential images recorded with about 4-min scan times.

When the level of $CaCl_2$ began to rise in the fluid cell, many of the BMV particles detached from the mica and were lost to observation. Some remaining particles in the field, identifiable in sequential scans because of their relative dispositions, are marked. The diameters of these particles were measured over the next 20 min. As shown in Table 2 and qualitatively apparent by inspection alone, the diameters of the particles decreased from 27–29 nm in (b) to 17–19 nm in (f). The progression shows that a direct transition from $T = 3$ to $T = 1$ particles is possible without complete dissociation of the capsid protein units.

We saw no emergence of RNA from the $T = 3$ particles during the transition, but we would not visualize the RNA by AFM unless it adhered stably to the mica. What is seen, however, is a substantial accumulation of material on the mica surface in the neighborhoods of the particles. From previous experience with other systems, we judged this most probably to be protein. In Fig. 10 is a high-resolution AFM image of this background material on the mica surface. While it appears largely amorphous, it can nonetheless be seen to be composed of discrete, roughly circular elements. The circular units have a depression or hole at their centers, giving them the appearance of toroids. We suspect that these are $T = 3$ capsomeres, predominantly hexamers, that have been cast off intact in the $T = 3$ to $T = 1$ transition and that the background protein is their accumulated mass.

QELS observations

Attempts to monitor the dissociation and reassembly process using QELS was not particularly successful. BMV particles (28 nm) were clearly identified as the only species significantly present at the beginning. Upon addition of $CaCl_2$, these dissociated almost immediately into a broad distribution of lower molecular weight products, in the size range of capsid protein oligomers and subunits. Shortly thereafter, however, reaggregation began and a great variety of peaks appeared in the range of 5 to 100 nm. These peaks constantly changed and shifted with time, suggesting active processes of assembly, disassembly, and rearrangement were occurring. This is probably not surprising given the great variety of structures and particles that BMV protein has been shown to form, including tubes, beads, and both large and small anomalous particles (Bancroft and Hiebert, 1967; Bancroft *et al.,* 1967; Pfeiffer *et al.,* 1976). We were not able to unambiguously identify any of these intermediate structures in our QELS experiments but presume a number of transient forms were present. In any case, the QELS results indicate that $T = 1$ particle formation can occur by means other than direct condensation of $T = 3$ particles. It suggests that dissociation to free oligomers and reassembly into higher molecular weight forms also occurs.

CONCLUSIONS

A variety of crystal forms of BMV can be obtained by vapor diffusion methods using PEG-MME 550 as the precipitant, and under otherwise similar conditions of pH, ionic strength, and temperature. In many cases different crystal forms are found to coexist within a single crystallization sample. The crystals do not appear to transform from one to another, suggesting that they do not simply represent metastable forms. More likely they arise from BMV particles that vary slightly among themselves in structure or some physical–chemical property. Certainly this observation, along with a host of others from diverse laboratories, suggests that BMV virions are malleable, variable in structure, or dynamic in their properties. This is consistent, also, with the poor-to-moderate diffraction properties of the crystals of BMV, a feature which can probably be ascribed to particle variability rather than defects in the crystals. Although the crystals of the $T = 3$ particles of BMV contain many absences and vacant lattice sites, they are not excessive when compared with other protein and virus crystals we have studied by AFM (Kuznetsov *et al.,* 2000; McPherson *et al.,* 2000). In addition, the BMV crystals appear virtually free of stacking faults and screw dislocations, defects which are responsible for the introduction of most long-range disorder in crystalline lattices.

The sources of many of the defects, holes, and absences that do appear in the AFM images of the crystal surfaces are interesting and are somewhat unique to virus crystals. Both anomalous smaller particles and anomalous larger particles are incorporated into the crystal lattices. These are seen to produce local disorder and the exclusion of some normal virions from neighboring lattice sites, thereby producing absences and holes. The smaller particles are almost certainly the $T = 1$ icosahedral particles (which were ultimately crystallized) derived from the $T = 3$ BMV virions. The larger particles could be double-shelled virions (Bancroft and Hiebert, 1967; Bancroft *et al.,* 1967), but we have no firm evidence for this. They might well be some other aberrant architecture. One implication of these observations is that anomalous particles, both smaller and larger than the normal virions, must also be naturally present in standard preparations of BMV. Furthermore, their surfaces must be sufficiently similar to those of normal BMV virions that they can be imperfectly accommodated in the lattices of crystals of the normal particles. Because they are so similar in the interactions they make with neighbors, yet are otherwise "not quite right," they are a major impurity in virus crystallization and a pervasive source of defects.

We show here that $T = 1$ particles of BMV can be produced from the normal $T = 3$ virions by exposure to high concentrations of $CaCl_2$, and they can subsequently be crystallized from 2.1 M sodium malonate. The results show that formation of $T = 1$ BMV particles occurs concomitant with proteolytic cleavage of the amino-terminal 35 amino acids, which leaves an amino-terminal alanine 36.

It is noteworthy that previous studies by Cuillel *et al.* (1981) of the formation of $T = 1$ BMV particles by $CaCl_2$ treatment utilized the addition of trypsin to the dissociated protein. This produced cleavage of the coat protein between amino acids 64 and 65 to produce a new terminal alanine 65. In the investigation presented here, an endogenous protease cleaves the polypeptide between amino acid 35 and 36, thereby increasing the length of the coat polypeptide necessary for $T = 1$ particle formation by 29 amino acid residues.

The amino-terminal peptides of viral coat protein subunits generally contain numerous basic amino acids which are thought to interact strongly with the negatively charged, encapsidated nucleic acid. Indeed, these peptides are generally observed by X-ray crystallography to disappear on the interior of virions and to be statistically disordered as they interact with RNA. It is suggestive that when RNase A is present, upon treatment with $CaCl_2$, the cleavage of the coat protein appears to occur more rapidly than in its absence. It may be that interaction between the protein and RNA protects the polypeptide to some extent from proteolytic attack. RNase A degradation of the nucleic acid may lead to increased exposure of the protein, and accelerated cleavage. If this is true, then it is evidence of significant interactions between the capsid protein of BMV and the encapsidated RNA.

Formation of $T = 1$ particles may occur by more than one mechanism, including reassembly of dissociated protein as suggested by QELS results. We do, however, see by AFM a direct condensation of $T = 3$ virions to $T = 1$ particles without apparent disassembly. This process is accompanied by the accumulation of substantial protein material on the mica substrate. Imaging of this protein material at higher resolution suggests that it may be composed of more or less intact capsomeres. Presumably these capsomeres are the hexameric units which must be shed to create a $T = 1$ particle. The continued presence of pentameric and hexameric capsomeres after disruption of the $T = 3$ particles and formation of $T = 1$ particles at high ionic strength attests to the stability and physical integrity of these structural units. These units are a product of disassembly, but their stability also suggests they may be intermediates in virus assembly as well.

The $T = 1$ particles visualized by AFM have a very distinctive appearance with their prominent, protruding pentameric capsomeres. They are, in appearance, quite unlike the satellite viruses which constitute the naturally occurring $T = 1$ virions in plants (Ban *et al.,* 1995). The particles and their crystals are quite stable and stand up well to manipulation, AFM, and X-ray data collection. The crystals of the $T = 3$ and $T = 1$ particles of BMV, as

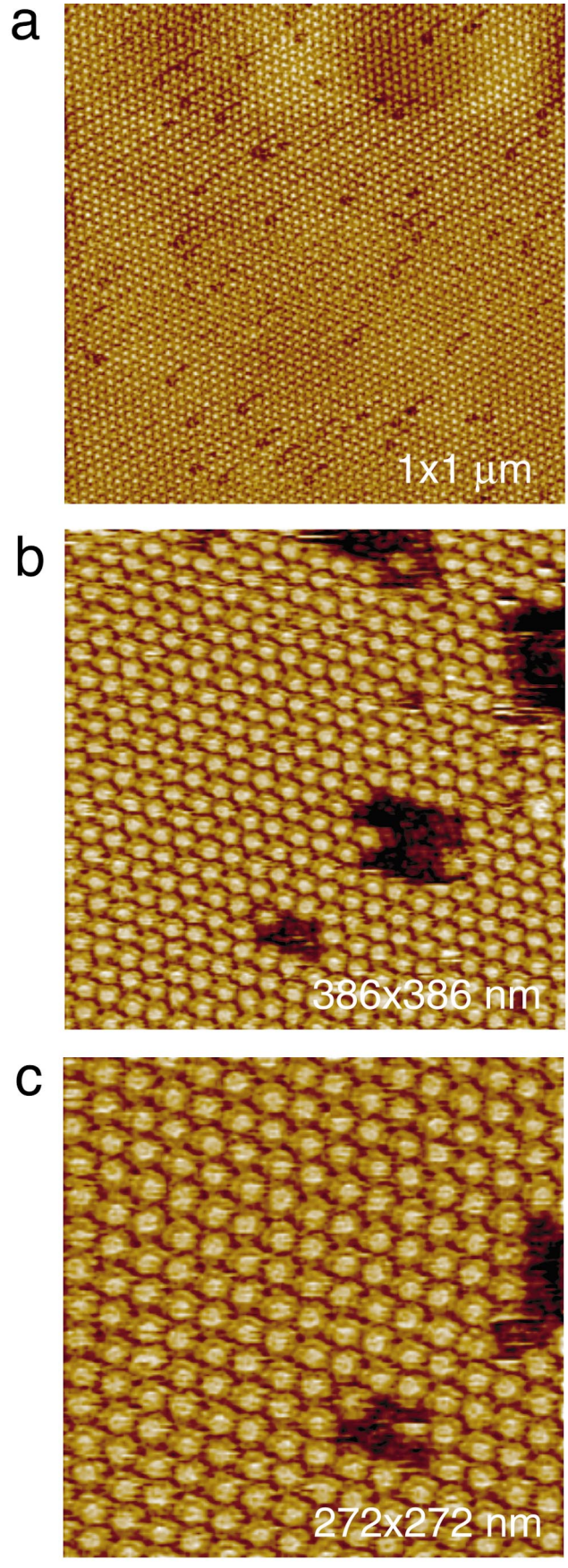

visualized by AFM, are about equal in their apparent degrees of perfection. Both exhibit a vast number of point defects or vacancies, but neither shows any evidence of screw dislocations or stacking faults (Malkin *et al.,* 1995, 1996). Despite this, the crystals of the $T = 1$ particles diffract to substantially higher resolution than do any of the three crystal forms of the $T = 3$ particles. This is true both at room temperature and under cryogenic conditions.

It seems probable that the higher resolution of the $T = 1$ particle crystals may be due to either (a) the $T = 1$ particles being more structurally uniform than the $T = 3$ particles, even though the former are created artificially, while the latter occur naturally; or (b) the orientations and dispositions of the $T = 1$ particles in their lattice are more secure and uniform than for the $T = 3$ particles in their crystals.

Though by no means definitive, two observations argue against the second choice as the cause of the difference in diffraction resolutions. First, based on virus particle volume, there is less solvent per $T = 3$ particle in its crystals than for a $T = 1$ particle in its crystal. Second, for none of three different crystal forms of the native virus particle, all having different packing arrangements, does the diffraction resolution approach that of the single crystal form of the $T = 1$ particles. Hence, we are inclined toward the first explanation, that the $T = 1$ particles are simply more ordered and uniform in structure than are native virus particles. This might well be a consequence of the elimination of the amino-terminal 35 amino acids, which are likely disordered in the native virions, as in most icosahedral plant viruses.

Finally, the results show that AFM is capable of producing quite respectable images of virus particles, even the smallest of the viruses, the $T = 1$ particles. Although not yet competitive with X-ray diffraction in resolution, it proves itself a worthy instrument for observing dynamic processes and changes confined to a two-dimensional plane.

MATERIALS AND METHODS

BMV purification

Barley plants (*H. vulgare* cv. Dickson) were infected with BMV (provided by A. L. Rao, UC Riverside) and virus was purified by a modification of the method of Rao (Adolph, 1994). Infected leaves were harvested and ho-

FIG. 8. In (a) through (c) are successively higher magnification AFM images of the surface of a tetragonal crystal of the $T = 1$ BMV particles. At high magnification, the capsomere structure of the $T = 1$ particles becomes apparent. The scatter of single absences and larger vacancies over the surface of the crystal is comparable to that seen in the native $T = 3$ BMV crystals and, therefore, is unlikely the cause of the substantial difference in the quality of the diffraction patterns of the two kinds of crystals.

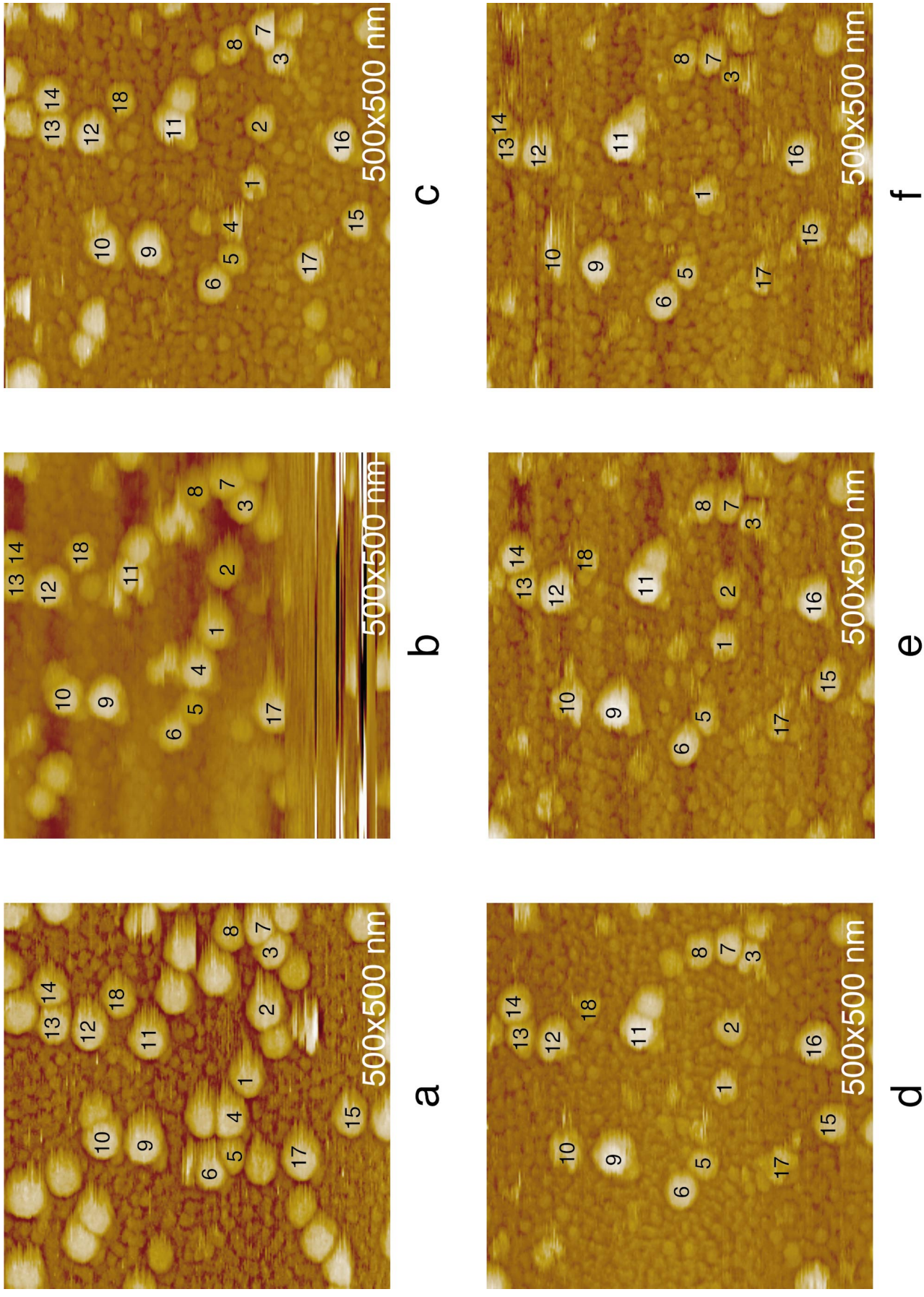
500x500 nm
a
500x500 nm
b
500x500 nm
c
500x500 nm
d
500x500 nm
e
500x500 nm
f

mogenized for 10 min at 4°C using a Waring blender with two parts extraction buffer (0.5 M sodium acetate, 80 mM magnesium acetate, and 1% β-mercaptoethanol) to one part plant tissue. After pressing through cheesecloth, the crude extract was clarified at 20,000 *g* in a GSA rotor for 20 min. PEG 8000 was added to the extract to 10% w/v and the solution was stirred overnight at 4°C. Virus was separated from the solution by centrifuging 20 min at 20,000 *g*. The pellet was resuspended in 1/10 diluted extraction buffer and allowed to stand overnight. These steps were then repeated a second time using 15% w/v PEG 8000. Virus was further purified by centrifugation on a $CsCl_2$ gradient with a refractive index of about 1.36 for 24 h in a Beckman SW41 rotor at 35,000 rpm. The opaque milky-white virus solution was visible by inspection and was removed by inserting a syringe into the side of the tube. After dialysis in 1/10 diluted extraction buffer overnight, the virus was concentrated to about 7 mg/ml for crystallization.

BMV $T = 1$ particles and BMV capsid protein

$T = 1$ icosahedral BMV particles, and free BMV protein, were produced by a modification of a conventional procedure (Choi *et al.,* 2000; Zhao *et al.,* 1995), but by omitting treatment with trypsin or any other proteases. Purified BMV along with 1 mg/ml RNase A was dialyzed overnight against 0.05 M Tris, 0.5 M $CaCl_2$, 1 mM DTT, at pH 7.5. The BMV coat protein solution was then dialyzed for 2 h against 20 mM Tris pH 7.5, 1.0 M NaCl, and 1 mM DTT for 2 h and centrifuged for 15 min at 4°C. The protein solution was then concentrated to 3 mg/ml prior to crystallization.

SDS–PAGE was conducted on intact virus and virus protein according to Laemmli (1970). Mass spectrometry was carried out on both native BMV virions and those treated with $CaCl_2$ as above to produce the $T = 1$ particles. This was performed by the UCI Protein Chemistry Facility using a PerSeptive Voyager DE PRO MALDI-TOF. Samples were dialyzed vs distilled water for 24 h before application. Amino-terminal sequencing was also carried out by the UCI facility using a Hewlett–Packard 6100 SA Protein Sequencer.

Crystallization

Crystals of both native $T = 3$ BMV, and the $T = 1$ particles prepared as above, were grown by vapor diffusion in Cryschem plates (Hampton Research, Laguna Niguel, CA) at room temperature. The particular polymorph of native BMV crystals that was obtained in a particular set of trials was difficult to predict, as crystallization appeared to be very sensitive to the history and handling of the sample, and virtually imperceptible changes in chemical and physical conditions. Frequently, different polymorphs were grown under the same conditions, and often multiple polymorphs were observed in the same crystallization sample. In general, however, crystals of intact BMV were reproducibly grown by mixing equal volumes of a reservoir containing 23% PEG-MME 550 and 0.1 M magnesium acetate at pH 5.2 with 7 mg/ml virus solution to produce crystallization drops of 20 μl volume. The drops were equilibrated through the vapor phase with 1.0 ml reservoirs in cells sealed with clear plastic tape.

After a screen of salt concentration and pH, crystals of $T = 1$ BMV particles were grown by vapor diffusion as above. In this case, however, the reservoir solution was 2.1 M sodium malonate at pH 7.5 (McPherson, 2001). The drops were composed of equal portions of the $T = 1$ virus solutions and the 2.1 M sodium malonate.

Data collection

Preliminary X-ray diffraction data were collected on all crystal forms at either the Advanced Light Source (Berkeley, CA) or Stanford Synchrotron Radiation Laboratory (Stanford, CA) using $\lambda = 1.1$ Å radiation. Data were processed using DENZO and SCALEPACK (Otwinowski, 1993). Data collection for two crystal forms could only be obtained at room temperature, while those for the remainder were obtained at cryogenic temperature. For the rhombohedral $T = 3$ crystals, flash cooling was accomplished by soaking about 60 s in 1 part mother liquor, 1 part glycerol, and 1 part PEG 400 along with excess solid sucrose. The high malonate concentration of the $T = 1$ particle crystals sufficed as cryogen, although all crystals investigated at −173°C were washed thoroughly through peritone oil prior to flash cooling.

AFM

The measurement of particle size and the dimensions of features of individual particles were treated with some care. Sizes of individual particles adsorbed to the mica appear considerably larger in their lateral dimension

FIG. 9. An experiment showing the transition of individual $T = 3$ BMV particles to $T = 1$ particles upon exposure to $CaCl_2$. In (a) is an AFM image of $T = 3$ particles adsorbed to freshly cleaved mica in buffer, in the fluid cell. The average height of the particles is 26 nm. In the top portion of (b) is a similar area showing the $T = 3$ particles but the interference at the bottom occurs as the $CaCl_2$ is injected into the fluid cell. Some particles detach from the mica and are lost at various times during the course of observation, but those marked by numbers remain attached to the mica substrate and permit measurement of their heights. Heights, which reflect the actual diameters of the particles as a function of time, are shown in Table 2. In progressing from (c) to (f) the heights decline from 28 nm to an average diameter of 18 nm, the diameters of the $T = 1$ particles. It should be remarked that the mica substrate, in addition to the viral particles, also contains a heavy accumulation of small, proteinaceous units, presumably portions of the capsids that are cast off during the transition. There is no evidence of viral RNA in the images at any time.

TABLE 2

Height Measurements of BMV Particles in Nanometers

Particle	−4 min	$CaCl_2$ added	+4 min	+8 min	+12 min	+16 min
1	25.0	24.4	20.9	19.9	14.4	19.1
2	30.4	21.9	19.8	19.2	15.6	
3	27.3	25.1	23.1	19.6	16.5	16.2
4	27.2	25.0	23.5	16.3		
5	21.0	16.3	15.8	16.2	15.6	16.4
6	27.2	21.8	20.9	21.5	20.7	21.3
7	28.9	24.5	27.8	21.6	16.8	18.0
8	22.0	20.9	18.7	18.2	16.6	15.3
9	30.3	30.4	18.7	18.2	16.6	15.3
10	27.8	27.1	26.3	22.0	20.9	18.5
11	27.2	27.2	29.9	28.6	27.0	27.7
12	26.3	27.2	26.5	26.0	24.9	18.2
13	25.3	23.0	23.6	20.3	18.2	17.3
14	23.7	21.3	22.5	22.8	19.6	17.3
15	24.9		22.2	22.8	18.5	17.9
16			28.4	26.6	25.6	22.3
17	28.4	27.2	24.6	15.8	13.2	15.9
18	21.7	21.6	17.4	14.9	12.0	
Avg.	26.2	24.1	22.8	20.6	18.4	18.4

because the image obtained is the convolution of the AFM tip shape with that of the particle. The tip is not infinitesimally sharp and its curved surface immediately adjacent to the absolute tip causes vertical displacement of the cantilever and, therefore, gives rise to edges in the image before as well as after the absolute tip encounters the object. This does not, however, affect the total vertical displacement of the cantilever. As a consequence, single objects visualized by AFM appear broader than their true dimensions, but yield an accurate and precise vertical dimension. For roughly spherical particles, such as icosahedral viruses, their diameters appear about 2.5 times greater than is in fact the case; however, the vertical "height" of particles provides a remarkably accurate value (within a few percent) for their true diameter. This was confirmed by measuring center-to-center distances of particles in crystalline lattices of the viruses when available, and by comparison with the detailed structures known from X-ray diffraction, light scattering, or electron microscopy. Therefore, particle sizes based on AFM of isolated particles cited here are based only on vertical measures of their diameters.

In the case of crystals, the situation is different. With virus crystals, each virion is embedded in a lattice composed of identical particles. As the AFM tip passes over the surface, the tip never approaches the "bottom" of a virion (i.e., a surface equivalent to the flat mica substrate) before it encounters a neighboring virion. Thus the heights of particles in crystals does not give a valid measure of their diameter. However, it is straightforward to measure center-to-center distances of the virus particles in the lattices, and because the particles are close packed, these distances yield an accurate and precise diameter, also to within a few percent of values deduced by X-ray diffraction or electron microscopy. Fourier transform of the lattice arrays in fact improve these values to better than 1 nm.

The most detailed images of virus particles are usually obtained from virus crystals rather than from single, free particles adsorbed to mica or glass. This is not due to any averaging process or Fourier filtering, but is an inherent property of the technique. Presumably the immobilization of the particles and their physical stability is responsible for the quality of the crystals' images. Unless otherwise explicitly stated, all AFM examinations were carried out in aqueous solutions in which virus crystals were stable.

For AFM visualization of individual viruses and $T = 1$ particles, samples were adsorbed onto freshly cleaved mica and examined both in air and in their mother liquor in sealed fluid cells. Crystals grown *ex situ* were transferred to sealed fluid cells of about 60 μl volume, fixed to the glass substrate by pinning them beneath fine glass fibers, and examined under solutions identical to their mother liquors, including virus. All operations were carried out at 22°C. The AFM instrument was a Digital Nanoscope III (Digital Instruments, Santa Barbara, CA) and images were collected in tapping mode using oxide-sharpened silicon nitride tips. Most procedures were those described earlier (Kuznetsov *et al.,* 1997, 2000; Malkin *et al.,* 1999b).

Quasi elastic light scattering measurements on the dissociation and reassociation of BMV virions was carried out using a Malvern 4700 c submicroparticle analyzer (Malvern Instruments, Inc., Southborough, MA) as described for earlier QELS investigations (Malkin *et al.,*

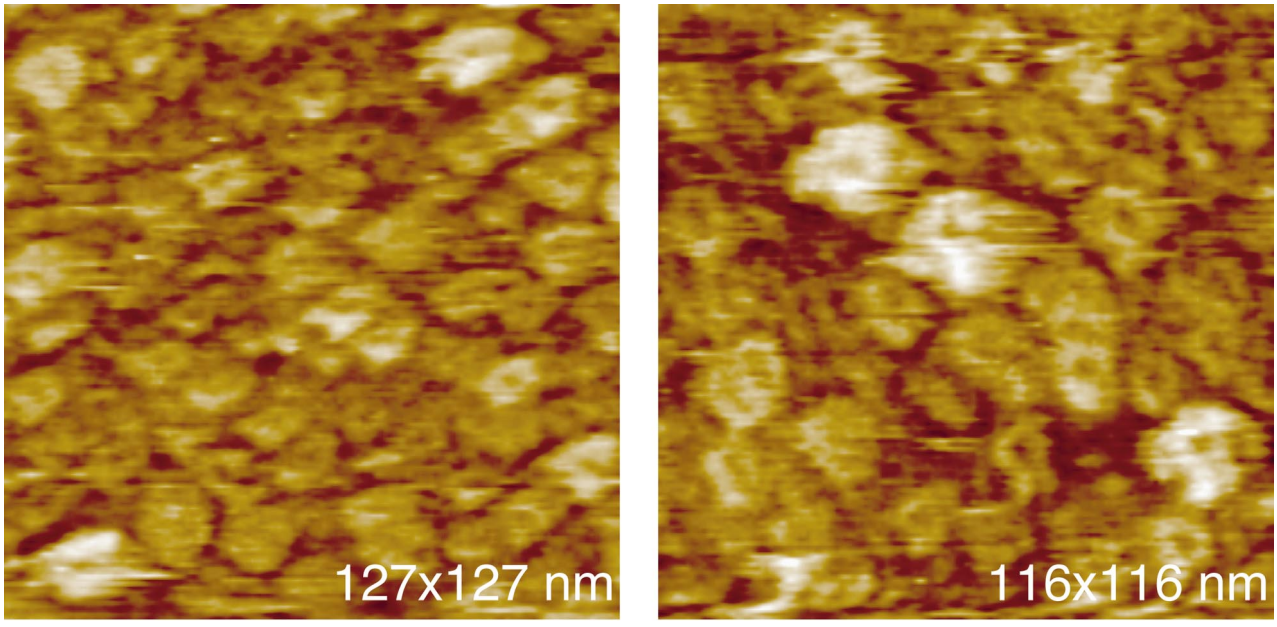

FIG. 10. High-resolution AFM images of the background material produced as a consequence of the $CaCl_2$-induced transition of the $T = 3$ to $T = 1$ particles, and which is adsorbed to the mica surface. It is apparent, even in these indistinct images, that the material is composed of individual toroid units of a size roughly consistent with the capsomeric units of the virions. In most units, an indentation, or hole, at the center is visible.

1993; Malkin and McPherson, 1993, 1994). The photomultiplier was always at 90° to the incident laser beam produced by an Innova 70-3, 1 W argon laser. All samples were centrifuged and passed through 0.22-μm syringe filters to remove large aggregates. Samples were of 50 μl volume and were contained in quartz microcuvettes (Starna Cells, Inc., Atascadero, CA).

ACKNOWLEDGMENTS

The authors gratefully acknowledge the technical assistance of Aaron Greenwood. This research was supported by contracts from the National Aeronautics Space Administration and a grant from the National Institutes of Health.

REFERENCES

Adolph, K. W. (1994). "Molecular Virology Techniques." Academic Press, San Diego.

Argos, P., and Johnson, J. E. (1984). Chemical stability in simple spherical plant viruses, in biological macromolecules and assemblies. *In* "Virus Structures" (F. A. Jurnak, and A. McPherson, Eds.), Vol 1. Wiley, New York.

Ban, N., Larson, S. B., and McPherson, A. (1995). Structural comparison of the plant satellite viruses. *Virology* **214,** 571–583.

Bancroft, J. B. (1971). Cowpea Chlorotic Mottle Virus. *CMI/AAB Descriptions of Plant Viruses*, pp. 49–52.

Bancroft, J. B., and Hiebert, E. (1967). Formation of an infectious nucleoprotein from protein and nucleic acid isolated from a small spherical virus. *Virology*, **32,** 354–356.

Bancroft, J. B., Hiebert, E., and Bracker, C. E. (1969). The effects of various polyanions on shell formation of some spherical viruses. *Virology*, **39,** 924–930.

Bancroft, J. B., Hills, G. J., and Markham, R. (1967). A study of the self-assembly process in a small spherical virus. Formation of organized structures from protein subunits in vitro. *Virology*, **31,** 354–379.

Bancroft, J. B., and Horne, R. W., Eds. (1977). Bromovirus (brome mosaic virus) group. *In* "Atlas of Insect and Plant Viruses" (Maramorosch, K., Ed.), Vol. 8, pp. 354–379, Academic Press, New York.

Choi, Y. G., Grantham, G. L., and Rao, A. L. (2000). Molecular studies on bromovirus capsid protein. *Virology* **270,** 377–385.

Cuillel, M., Jacrot, B., and Zulauf, M. (1981). A $T = 1$ capsid formed by the protein of brome mosaic virus in the presence of trypsin. *Virology* **110,** 63–72.

Krol, M. A., Olson, N. H., Tate, J., Johnson, J. E., Baker, T. S., and Ahlquist, P. (1999). RNA-controlled polymorphism in the *in vivo* assembly of 180-subunit and 120-subunit virions from a single capsid protein. *Proc. Natl. Acad. Sci. USA* **96,** 13650–13655.

Kuznetsov, Y., G., Malkin, A. J., and McPherson, A. (2000). Atomic force microscopy studies of icosahedral virus crystal growth. *Colloids Surf* **19,** 333–346.

Kuznetsov, Y. G., Malkin, A. J., Land, T. A., DeYoreo, J. J., Barba, A. P., and McPherson, A. (1997). Molecular resolution imaging of macromolecular crystals by atomic force microscopy. *Biophys. J.* **72,** 2357–2364.

Laemmli, U. K. (1970). Cleavage of structural proteins during the assembly of the head of bacteriophage T4. *Nature,* **227**(259):680–685.

Lane, L. C. (1981). The bromoviruses. *In* "Handbook of Plant Virus Infection and Comparative Diagnosis" (E. Kurstak, Ed.), Elsevier, North-Holland, Amsterdam.

Malkin, A., Kuznetsov, Y., Lucas, R., and McPherson, A. (1999a). Surface processes in the crystallization of turnip yellow mosaic virus visualized by atomic force microscopy. *J. Struct. Biol.* **127**(N1), 35–43.

Malkin, A. J., Cheung, J., and McPherson, A. (1993). Crystallization of satellite tobacco mosaic virus. I. Nucleation phenomena. *J. Cryst. Growth* **126,** 544–554.

Malkin, A. J., Kuznetsov, Y. G., Land, T. A., DeYoreo, J. J., and McPherson, A. (1995). Mechanisms of growth for protein and virus crystals. *Nat. Struct. Biol.* **2,** 956–959.

Malkin, A. J., Kuznetsov, Y. G., and McPherson, A. (1999b). *In situ* atomic

force microscopy studies of surface morphology, growth kinetics, defect structure and dissolution in macromolecular crystallization. *J. Cryst. Growth* **196,** 471–488.

Malkin, A. J., Kuznetsov, Y. G., and McPherson, A. (1996). Defect structure of macromolecular crystals. *J. Struct. Biol.* **117,** 124–137.

Malkin, A. J., and McPherson, A. (1994). Light scattering investigations of nucleation processes and kinetics of crystallization in macromolecular systems. *Acta Cryst. D* **50**, 385–395.

Malkin, A. J., and McPherson, A. (1993). Light scattering investigations of protein and virus crystal growth: Ferritin, apoferritin and satellite tobacco mosaic virus. *J. Cryst. Growth* **128,** 1232–1235.

McPherson, A. (2001). A comparison of salts for the crystallization of macromolecules. *Protein Sci.* **10,** 418–422.

McPherson, A., Malkin, A. J., and Kuznetsov, Y. G. (2000). Atomic force microscopy in the study of macromolecular crystal growth. *Annu. Rev. Biophys. Biomol. Struct.* **29**, 361–410.

Nicholls, A., Sharp, K., and Honig, B. (1991). Protein folding and association-insights from the interfacial and thermodynamic properties of hydrocarbons. *Proteins Struct. Funct. Genet.* **11,** 281–296.

Otwinowski, Z. and Minor, W. (1997). Processing of X-ray diffraction data collected in oscillation mode. *In* "Methods in Enzymology, Macromolecular Crystallography" (Carter, C. W. Jr., Sweet, R. M., Eds.) vol. 276, pp. 307–326, Academic Press, New York.

Pfeiffer, P., Herzog, M., and Hirth, L. (1976). RNA viruses: Stabilization of brome mosaic virus. *Philos. Trans. R. Soc. Lond. B Biol. Sci.* **276,** 99–107.

Pfeiffer, P., and Hirth, L. (1974). Aggregation states of brome mosaic virus protein. *Virology* **61,** 160–167.

Pirone, T. P., and Shaw, J. G. (1990). "Viral Genes and Plant Pathogenesis." Springer-Verlag, Berlin/New York.

Van Regenmortel, M. H. V., Fauquet, C. M., and Bishop, D. H. L. (1999). "Virus Taxonomy: Seventh Report of the International Committee on Taxonomy of Viruses." Academic Press, San Diego, CA; London.

Zhao, X., Fox, J. M., Olson, N. H., Baker, T. S., and Young, M. J. (1995). *In vitro* assembly of cowpea chlorotic mottle virus from coat protein expressed in *Escherichia coli* and *in vitro* transcribed viral cDNA. *Virology* **207,**.